Applied Physics A (2023) 129:716
https://doi.org/10.1007/s00339-023-06974-7

Applied Physics A
Materials Science & Processing

Magnetic relaxation in epitaxial films with in-plane and out-of-plane anisotropies

Abdellah Lisfi[1] · Frank Efe[1] · Manfred Wuttig[2]

Received: 19 May 2023 / Accepted: 25 August 2023

Abstract
Nanomagnetic materials are needed for increasing data storage capacity and suited for enhancing the performance of permanent magnets. However, their performance is controlled by magnetic switching, which is driven by a competition between thermal activation energies and anisotropy energies. Here, we elucidate the magnetic switching process in epitaxial films with in-plane and out-of-plane magnetic anisotropies. While in both media the magnetization obeys a logarithmic decay over time, a drastic difference is revealed in their magnetic viscosities. The relaxation logarithmic law is a consequence of the epitaxy itself under which the film growth is initiated through random nucleation followed by islands growth and their coalescence, leading to non-uniform structural domains. These structural domains behave like magnetic domains due to the presence of antiphase boundaries where exchange coupling is disrupted. The activation volume for both media is found to match the average size of the structural domains. The very slow relaxation process under out-of-plane anisotropy is linked to the demagnetizing field, which drastically weakens the irreversible magnetic susceptibility. A simple analytical model was developed and found to well predict and corroborate the experimental findings. This study was conducted on $CoFe_2O_4$ films epitaxially grown on (100) and (110) MgO substrates.

Keywords Magnetic anisotropy · Magnetic relaxation · Epitaxial films · Antiphase boundaries

1 Introduction

Magnetic relaxation is a thermally activated irreversible process that occurs in ferromagnets [1–5] due to the unstable character of their magnetization, which can switch between its energetically favorable metastable states (see Fig. 1). It is of a considerable interest to permanent magnets application and data storage technology [6, 7]. Nano-sized magnetic materials are highly suited for enhancing the performances of permanent magnets through high coercivity and large energy product $(BH)_{max}$ due to their single magnetic domain character that can favor coherent rotation mode as mechanism of magnetization reversal [8, 9]. On the other hand, ultra-high recording densities storage requires magnetically decoupled nano-sized media with uniform grain size and narrow switching field distribution.

The characteristic time of the relaxation τ depends on the ratio between the energy barrier ΔE (difference between the maximum of energy and its minimum that holds the magnetization) and the thermal energy kT (k is the Boltzmann constant, and T is the absolute temperature of the ferromagnet) (see Fig. 1) according to the Arrhenius–Neel law $\tau = \tau_0 e^{\Delta E/KT}$ ($\tau_0 = 10^{-9}$ s) [1]. The energy barrier ΔE strongly depends on the magnitude of the external applied field and varies linearly with the volume V of the relaxing magnetic particle through the anisotropy energy $K_u V$ (K_u is the anisotropy constant of the particle). For an ideal system consisting of non-interacting particles media with a uniform size, the magnetization relaxes according to the equation $M(t) = M_0 e^{-t/\tau}$ (M_0 is the initial magnetization at the origin of time). However, for a magnetic system with a distribution of energy barriers related to magnetic domain-volumes distribution $f(V)$, the relaxation process is averaged over the whole volume distribution according to the equation $M(t) = \int M_0 e^{-t/\tau} f(V) dV$ [10]. This results into a new time dependence behavior of the magnetization described by $M(t) = C - S \times \ln(t)$, where

✉ Abdellah Lisfi
Abdellah.Lisfi@morgan.edu

[1] Department of Physics, Morgan State University, 1700 E. Cold Spring Lane, Baltimore, MD 21251, USA

[2] Department of Materials Science and Engineering, University of Maryland, College Park, MD 20742, USA

Published online: 20 September 2023

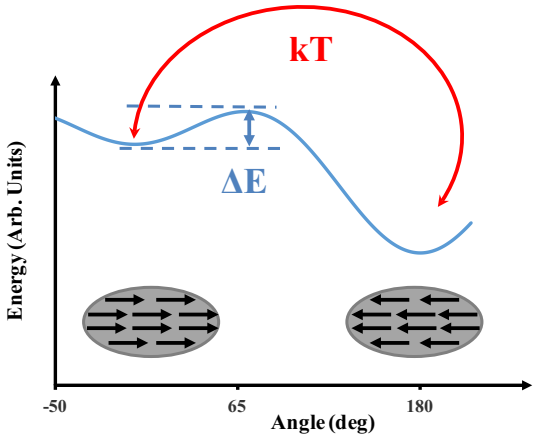

Fig. 1 Angular distribution of the free energy of uniaxial ferromagnet showing the two metastable states of the magnetization through the two minima of energy. Thermal switching can be activated if the thermal energy kT becomes competitive with the energy barrier ΔE, leading to an irreversible jump of the magnetization between its positively and negatively aligned directions

S is the magnetic viscosity of the ferromagnet and C is a constant known as the initial magnetization of the relaxation process. The magnetic viscosity S varies with the applied magnetic field and its maximum value is typically reached at the coercivity field due to the reduction in the energy barrier ΔE, which becomes zero. The mechanism of magnetic relaxation is reasonably understood in particulate and granular magnetic systems with either random or oriented magnetic anisotropy [11] due to abundant experimental and theoretical studies that have significantly advanced scientific knowledge in this field. However, the thermally activated switching processes of epitaxial structures have not been much investigated and the effects of the alignment of magnetic anisotropy on the relaxation process are not well established in two-dimensional structures.

In this paper, we investigate the magnetic relaxation process in epitaxial films with two different alignments of magnetic anisotropy (in-plane and out-of-plane) and we elucidate the mechanism behind the considerable reduction of magnetic viscosity in perpendicular media and their high thermal magnetic stability in comparison to those with in-plane aligned magnetic anisotropy. The study of interest was conducted on $CoFe_2O_4$ films epitaxially grown on (100) and (110) MgO substrates. The choice of $CoFe_2O_4$ for this relaxation study is motivated by its potential applications in magnetic and magneto-optic recordings [12] as well as its large magnetic anisotropy [13–15], which allows an accurate measurement of the magnetization irreversible process through the remanence curves. In the bulk phase, the magnetocrystalline anisotropy of cobalt ferrite is cubic and its first order K_1 is about 10^5 J/m^3 [14], whereas in epitaxial thin films of this magnetic oxide, the symmetry, the magnitude and the alignment of the anisotropy depend on the amount and the nature of strain (tension or compression) due to the domination of magnetoelastic effects [15]. The preference of MgO as a growth template is justified by its extremely small lattice mismatch with cobalt ferrite, which can easily promote an epitaxial film growth. Moreover, the uniqueness of cobalt ferrite for this investigation is reflected on the alignment of its magnetic anisotropy, which can be either parallel or perpendicular to the film plane depending on the crystallographic orientation of the MgO template [16, 17]. The synthesized (110) films display an in-plane magnetization easy axis, whereas the anisotropy is found to be oriented along the normal to the film plane for those deposited on (100) MgO. The study of interest is supported with results that include magnetic measurements (magnetization time dependence, hysteresis loops, remanence curves, and irreversible susceptibility), anisotropy measurement (torque curves), and structural analyses performed with X-ray diffraction (XRD) and transmission electron microscopy (TEM).

2 Experimental procedure and growth conditions of the films

The samples prepared for this study were fabricated by pulsed laser deposition (PLD) from polycrystalline $CoFe_2O_4$ target in well controlled growth conditions. The substrates used for the growth consist of one side polished MgO with (100) and (110) crystallographic orientations. The very small lattice mismatch between MgO and $CoFe_2O_4$ (0.48%) promotes MgO to be an excellent template for growing epitaxial cobalt ferrite films, where one $CoFe_2O_4$ lattice unit can fit on the top of four MgO lattice units. The film growth takes place in a vacuum chamber, where high purity oxygen is introduced when the pumping pressure reaches the threshold of 10^{-6} Torr. KrF excimer laser operating in the UV at 248 nm wavelength was used to irradiate the rotating $CoFe_2O_4$ target positioned at a constant distance (55 mm) from the substrate. The laser energy density on the target and its repetition rate were adjusted to 1.5 J/cm^2 and 3 Hz, respectively and maintained at these values during the deposition period. During the film growth, the substrate was heated at 300 °C and oxygen was supplied at a constant pressure. Under these conditions, the average deposition rate was 0.5 Å/s, and films with in-plane and out-of-plane magnetic anisotropies have been prepared on (110) and (100) MgO, respectively. It is important to note that the samples investigated in this study are 300 nm thick (~360 unit cells along the normal direction to the film plane) and display a perfect alignment of magnetic anisotropy as it will be revealed by structural and magnetic measurements. For all further details of the investigation, the films with in-plane

and out-of-plane anisotropies will be referred to as samples I and O, respectively.

3 Magnetic relaxation, magnetic viscosity and activation volume

The relaxation measurement (Fig. 2) was performed at room temperature with a vibrating sample magnetometer (VSM) along the magnetization easy axis, which is aligned in-plane and out-of-plane for samples I and O, respectively. The detail of the measurement is reported in [11]. Prior each measurement, a positive field of 20 kOe is initially applied to saturate the magnetization in the positive direction, then a constant negative is applied and maintained constant during the relaxation measurement, which takes about 2000s. It is important to note that the coercivity fields for both I and O samples mentioned in this section discussion were determined through hysteresis loops measurement detailed in Sect. 5. Figure 2a displays typical relaxation curves of sample O measured at three different fields (− 3.5 kOe, − 7.5 kOe and − 11.5 kOe). It is clearly demonstrated trough these relaxation graphs that under a perpendicular anisotropy, the magnetization manifests a slow decay over time for each applied field. This decay is a direct quantification of the magnetic switching driven by thermal activation in the film. Moreover, as well illustrated by the three graphs of Fig. 2a, this irreversible process exhibits a logarithmic character similar to that predicted in non-uniform size magnetic media. On the other hand, the slope of the magnetization decay known as the magnetic viscosity S is surprisingly small (1.6 kA/m) at the coercivity field ($H_c = -$ 6 kOe) in spite of a reduced energy barrier expected at this field. Additionally, S does not completely vanish at low and large fields (− 3.5 kOe and − 11.5 kOe) but instead displays a small value estimated at 1.3 kA/m, meaning that thermal relaxation is slow but still

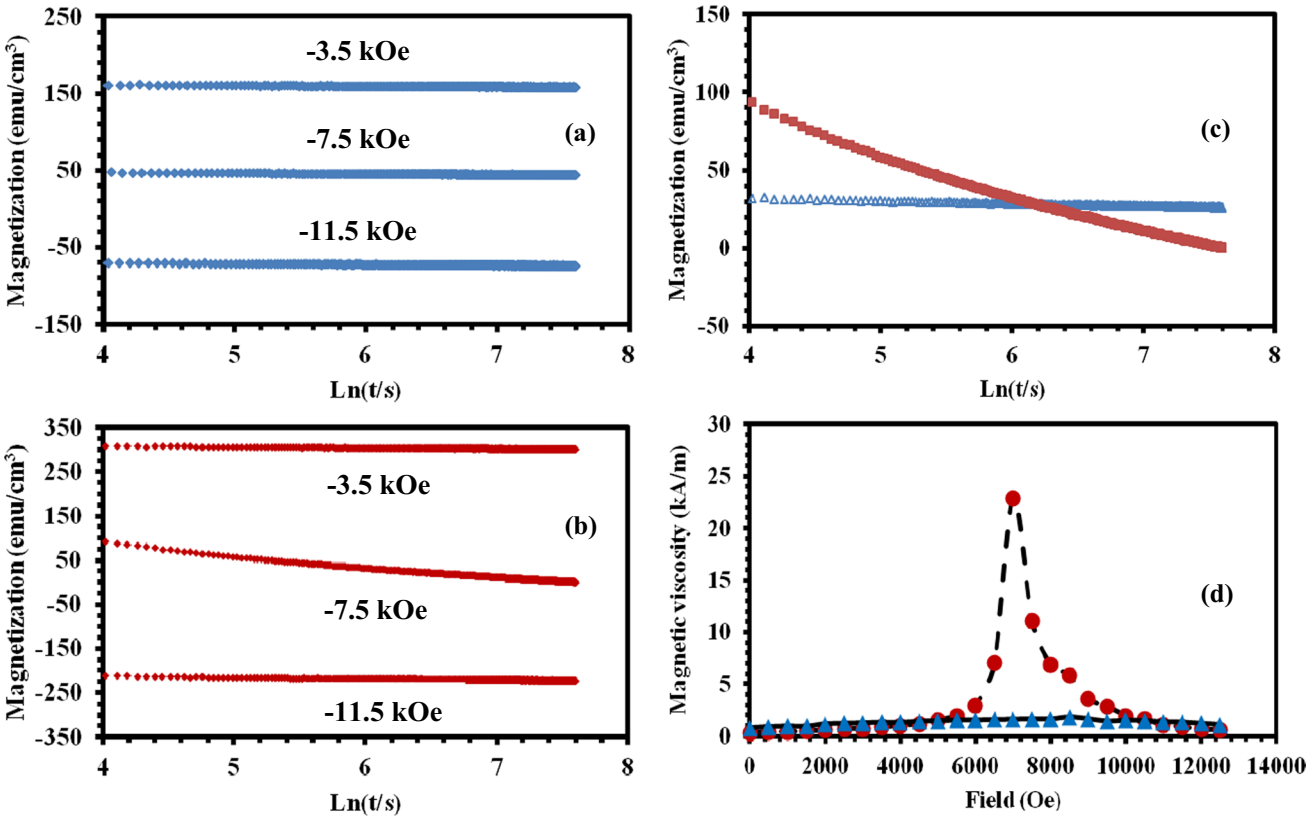

Fig. 2 Magnetization time dependence for epitaxial cobalt ferrite heterostructures with **a** out-of-plane and **b** in-plane aligned magnetic anisotropies, measured at three different applied fields (− 3.5 kOe, − 7.5 kOe and − 11.5 kOe) along their easy axes. Note that the magnetization decay over time obeys a logarithmic law regardless the alignment of the magnetic anisotropy. The slope of the magnetization decay over time is strongly dependent on the magnitude of the applied field for in-plane anisotropy (**b** graph), whereas it is almost constant with the field for out-of-plane film (**a** graph). **c** Time dependence behavior of the magnetization measured at the coercivity field where the energy barrier is expected to vanish for in-plane (red curve) and out-of-plane (blue graph) anisotropies. At the coercivity field, the relaxation process is much pronounced for in-plane media in comparison to the out-of-plane anisotropy film as illustrated by the slope of the magnetization decay. **d** Field dependence of the magnetic viscosity for in-plane (red circles curve) and out-of-plane (blue triangles curve) showing the strong dependence of the thermal stability on the magnetic anisotropy alignment

active in this field range. Figure 2b shows the relaxation curves of sample I with an in-plane easy axis measured at three different applied fields with magnitudes equal, smaller and larger than the coercivity field of the film of interest. As illustrated by the graphs of Fig. 2b, the magnetization time dependence under an in-plane anisotropy obeys the typical logarithmic law characteristic of uniaxial ferromagnets with a wide distribution of thermally active volumes. However, in contrast to extremely low magnetic viscosity S at low and large fields (− 3.5 kOe, and − 11.5 kOe), which remains under 1 kA/m, the magnetization relaxation at the coercivity field is very pronounced and its decay rate exceeds 22 kA/m. A direct comparison between the relaxation curves at the coercivity field for both samples O and I is depicted in Fig. 2c. It can be observed that although the thermally activated irreversible character of the magnetization is governed by the same logarithmic law in both samples (O and I), there is a drastic difference in the magnetization decay behavior related to the alignment of magnetic anisotropy. More precisely, at the coercivity field, the relaxation process quantified through the slope of the magnetization decay is more than fifteen times stronger under an in-plane anisotropy in comparison to the film with an out-of-plane easy axis. To better analyze the effects of the alignment of the magnetic anisotropy on the magnetic relaxation process, the field dependence of the magnetic viscosity is presented for both samples (I and O) in Fig. 2d. As illustrated by the dashed curve, under the control of an in-plane anisotropy the relaxation process is very active in narrow field range that extends from 6 to 10 kOe as demonstrated by the large magnetic viscosity that can exceed 22 kA/m at the coercivity field. However, outside this narrow applied field window, thermally activated relaxation vanishes due to the considerable reduction in the magnetic viscosity, which approaches zero. On the other hand, as depicted by the solid graph of Fig. 2d, under the control of an out-of-plane anisotropy, the magnetization is very stable over time regardless the magnitude of the applied field as demonstrated by the very slow magnetic relaxation where the maximum of magnetic viscosity remains under 2 kA/m. It is important to point out that outside the field range of 6–10 kOe, the relaxation process becomes less sensitive to the magnetization easy axis alignment since under both anisotropies (in-plane and out-of-plane) the magnetic viscosity is almost the same as illustrated by the two graphs of Fig. 2d, which are superimposed on the top of each other. The activation volume V_{ac} for these two relaxing structures was determined according to the equation $V_{ac} = (kT \times \chi_{irr})/(M_s \times S)$ [18, 19], where kT represents the thermal energy, χ_{irr} is the irreversible susceptibility, M_s is the saturation magnetization and S is the magnetic viscosity. V_{ac} was estimated to be 2.65×10^3 nm^3 and 3.43×10^3 nm^3 for in-plane and out-of-plane anisotropies, respectively. More precisely, the average in-plane diameter (D_{av}) of the active volume for the relaxation process was determined to be 13.8 nm and 15 nm for in-plane and out-of-plane anisotropies, respectively. It is interesting to note that there is an alternative experimental method for determining the activation volume for a relaxing magnetic system. This method is based on the measurement of the dependence of the coercivity H_c on the sweep rate of the applied field dH/dt [20]. The slope q of the predicted linear relationship between H_c and $\ln(dH/dt)$ is used to estimate the activation volume according to the equation $V_{ac} = kT/(q \times M_s)$. To better understand the thermally activated process in these two-dimensional structures, which is described by a logarithmic law and very stable magnetization in out-of-plane media as revealed by their slow relaxation process, it is imperative to pursue further investigations including structural characterization and magnetic measurement of both reversible and irreversible components of the magnetization. These investigations are further detailed in the next sections.

4 Structural analyses and domains imaging

Structural analyses through X-ray diffraction measurements are among the key results supporting this investigation as displayed by different scans of Fig. 3. The diffractometer used in this study is Philips PANanalytical X'Pert XRD System where the X-ray radiation is generated with a Cu anode. Figure 3 represents the XRD data for the film grown on (100) MgO. As illustrated by Fig. 3a, the $\theta/2\theta$ symmetric scan shows a highly oriented film due to the unique presence of textures parallel to (100). Moreover, the (400) film peak is shifted to high angles in comparison to the cubic bulk structure, indicating a lattice distortion where the lattice parameter along the normal axis to the film plane $a_\perp = 8.32$ Å is found to be smaller than the cubic lattice parameter $a_0 = 8.38$ Å. The presence of a peak shoulder with an intensity close to 50% of the major peak in the spectra is identified as the contribution of $K\alpha_2$ wavelength of the X-ray diffracting beam. However, the high resolution between $K\alpha_1$ and $K\alpha_2$ contributions illustrated by the spectra of Fig. 3a reveals a very uniformly distorted lattice in the film. The in-plane lattice parameter of the film was determined through XRD asymmetric scan measurement. In a such measurement, the scan geometry is modified by introducing an offset angle between the angles θ (angle between the incident X-ray beam and the film surface) and 2θ (angle between the incident X-ray beam and the detector) to uniquely allow specific oblique crystallographic planes such as (511) to diffract. The result of the asymmetric scan is displayed in Fig. 3b where the (511) texture is present in the spectra through a narrow peak (full width at the half maximum is less than 0.3°) localized at diffracting angle 2θ equals to 57.35°. By combining Bragg equations for symmetric and

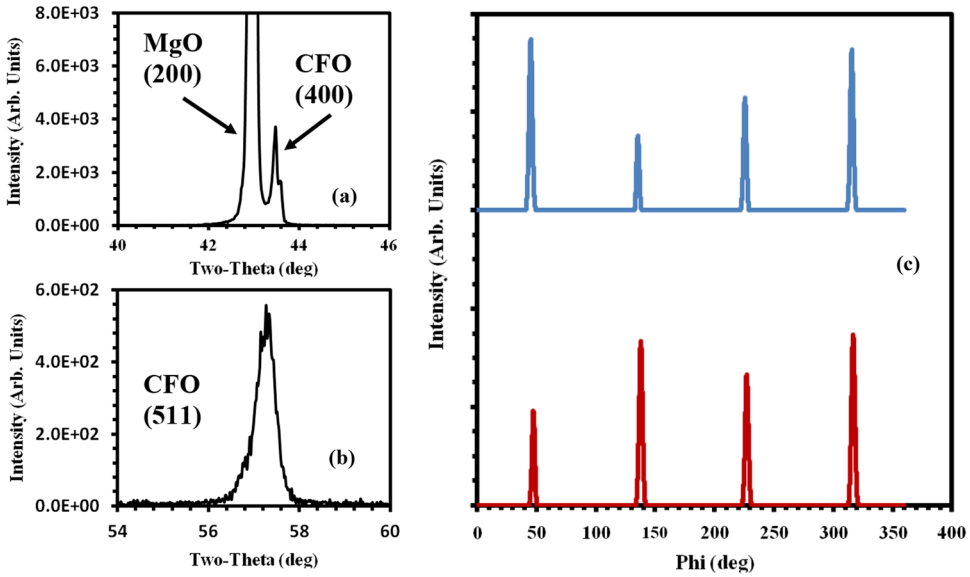

Fig. 3 XRD **a** symmetric and **b** asymmetric scans of $CoFe_2O_4$ film grown on (100) MgO substrate. Both scans reveal a highly oriented film with uniform tetragonal lattice distortion through the shift of the diffracting peaks and the presence of $K\alpha_1$ and $K\alpha_2$ peaks in the $\theta/2\theta$ scan spectra. **c** XRD Phi scan of the (511) texture showing the epitaxial nature of the (100) film through the perfect alignment of the peaks of the film (red curve on bottom) and the substrate (blue curve on top)

asymmetric scans, both in-plane and out-of-plane lattice parameters were determined ($a_{\perp}=8.32$ Å and $a_{//}=8.62$ Å) and used to estimate the lattice distortion factor (1.036), which is large enough for generating a strong uniaxial anisotropy for this ceramic film. To confirm whether the films are epitaxial or just oriented, XRD phi scan was performed on the synthesized films. For this study, the crystallographic plane of interest was (511) for $CoFe_2O_4$ and MgO. As illustrated by Fig. 3c the phi scan of (511) MgO displayed on top (blue line) shows a four-fold symmetry (four peaks equally separated from each other by 90°). The phi scan of cobalt ferrite on bottom (red line) exhibits the same symmetry and its four (511) peaks are perfectly aligned with those of MgO. This perfect matching of the two oblique (511) planes of the film and the substrate is a good illustration of the epitaxial nature of the film. It is important to point out that the XRD data for (110) films have not been included into this article due to the similarity between the results for (100) and (110) films, which both confirm an epitaxial structure with a tetragonal lattice distortion. It is important to point out that although XRD was powerful in revealing the epitaxial nature of these films, the reported discoveries about the relaxation process and the activation volume are still not understood and the following questions remain unanswered. (1) Why the magnetization time dependence in these epitaxial heterostructures obeys a logarithmic law? (2) Why the size of the activation volume is in the range of 13.8–15 nm? To answer these questions, we performed additional structural measurement based on nanostructure imaging with a transmission electron microscopy (TEM). A special chemical method for the TEM sample preparation has been developed to allow the high resolution imaging of the nanostructure with all its features. This method consists of dissolving the entire MgO substrate in 4 wt% $(NH_4)_2SO_4$ chemical solution, and pieces of the extracted Cobalt ferrite film were directly mounted on the microscope copper grids for TEM imaging. Figure 4 depicts typical HRTEM image of the epitaxial cobalt ferrite film, which reveals the following characteristics. (1) The films are textured mono crystals. (2) At the nano-metric scale, the structure is built of domains, which are delimited by boundaries (blue lines in the picture). (3) The shape and the size of these domains are not uniform. More precisely, the domain diameter varies between 5 and 30 nm. The irregularity in the domain shape and size is related to the growth mechanism which consists of island growth with random nucleation sites at early stage of the growth [21, 22]. The coalescence of the neighboring islands during the film growth leads to the formation of domains with different

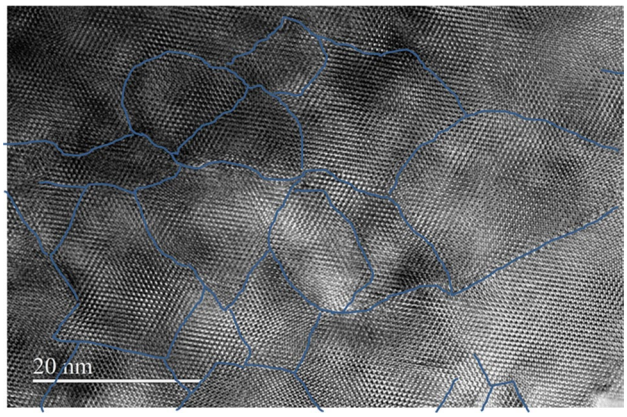

Fig. 4 HRTEM image of epitaxial cobalt ferrite film showing the monocrystalline structure of the film. At the nano-scale the film structure consists of domains with irregular shapes and non-uniform size which varies between 5 and 30 nm in diameter. The structural domains are delimited by anti-phase boundaries as shown by the blue lines

shapes and size. The domains are delimited by antiphase boundaries [23–25] (blue lines), which are structural defects where the unit cell is shifted within the monocrystalline structure. This shift in the unit cell is necessary for keeping the matching between the monocrystalline structure and the crystallographic symmetry of the film and those of the substrate. The magnetic exchange coupling is disrupted at the antiphase boundaries and the observed nanometric structural domains behave like magnetic domains. This very important result allows us to interpret the previous findings about the relaxation process and the activation domain. The epitaxial film of interest consists of decoupled magnetic domains with a non-uniform size. Each domain behaves like a single magnetic entity, where the magnetization can switch between its two energetically favorable metastable states as illustrated by Fig. 1. The magnetization switching for each domain is more likely to occur through coherent rotation due to the small domain size that cannot sustain multi-domain structure and to the large magnetic anisotropy of the heterostructure as it will be revealed by the magnetic characterization of the next section. The switching can be thermally activated and its average over the whole domain size distribution leads to a logarithmic dependence of the magnetization over time as previously established from the magnetic relaxation study. The activation volume estimated for both in-plane and out-of-plane media (13.8–15 nm) fits perfectly with the average domain size imaged with TEM. This suggests that the thermally active volume for the relaxation is the entire physical volume of the structural domain and the magnetization reversal mechanism is more likely to be controlled by coherent rotation mode. It is important to recognize the crucial role of the structural investigation in interpreting and understanding the relaxation process in these epitaxial heterostructures. However, the information learned from the nanostructure imaging is not helpful in determining the effects of the orientation of the magnetic anisotropy on the thermally activated switching of the magnetization and comprehending the large difference between the in-plane and the out-of-plane magnetic viscosities reported previously. Magnetic characterization including the measurement of the irreversible character of the magnetization is needed to clarify how magnetic viscosity is affected by the easy axis orientation, explain the slow relaxation process in out-of-plane media and establish a simple relationship between the in-plane and the out-of-plane viscosities.

5 Magnetic properties and irreversible magnetization processes

The magnetic characterization of the epitaxial films of interest has been performed through hysteresis loops measurement with a vibrating sample magnetometer (VSM) and anisotropy torque curves with a torque magnetometer (TMM). Figure 5 depicts the in-plane and the out-of-plane hysteresis loops as well as the torque curves for both (100) and (110) epitaxial films. As displayed by Fig. 5a, the out-of-plane anisotropy character of the (100) film is illustrated through the large perpendicular hysteresis loop (blue curve) in comparison to the small in-plane magnetization curve (red graph). Additional typical characteristics of the macroscopic magnetic properties of (100) film are revealed and summarized as follow. (1) With 22 kOe as maximum field for the VSM measurement, the hysteresis curves consist of major loops rather than minor loops. (2) The large hysteresis displayed by the perpendicular loop is a combination of a high coercivity field ($H_c \sim 6$ kOe) and a large remanence ($m_r \sim 0.8$). (3) The shearing of the perpendicular hysteresis loop is more likely to be produced by the demagnetizing field, which is generated by the out-of-plane measurement geometry. (4) The linear and reversible character of the in-plane magnetization curve with the exception of low field small hysteretic jump reveals that the film plane represents the hard axis of the magnetization. A linear extrapolation of the in-plane magnetization curve to high fields provides an estimation of the film anisotropy field H_k at the value of 40 kOe. It is important to point out that the anisotropy field represents an intrinsic property of the magnetic material in contrast to the coercivity field, which is controlled by other factors such as the material microstructure [26] and the magnetization reversal mechanism [27, 28]. Figure 5b depicts typical hysteresis loops of (110) films, which display the following magnetic characteristics. (1) The in-plane alignment of the magnetization easy axis is revealed through the large square magnetization curve (dashed red line) measured along [001]. (2) Both the coercivity field and the squareness displayed by this in-plane hysteresis loop are quite large ($H_c \sim 7500$ Oe, $S \sim 0.85$) and the switching between the two metastable states representing the magnetization saturation along the negative and the positive directions takes place in a narrow-applied field range. (3) The out-of-plane magnetization curve (solid blue line) exhibits a sheared hysteresis loop that closes at 10 kOe to become linear and reversible at larger fields. Extrapolating the linear character of the out-of-plane magnetization curve to very large fields allows the determination of the effective anisotropy field $H_{k,eff}$ to be 45 kOe. This gives an estimation of the anisotropy field H_k to be 40 kOe based on the saturation magnetization of the films ($M_s \sim 400$ emu/cm^3). Even though the magnitude of the anisotropy field is the same in both (100) and (110) films, significant differences can be observed through their magnetization curves measured along their respective easy axes. (1) The reduced remanence in the out-of-plane loop in (100) film is associated with the shearing induced by the demagnetizing field, which is insignificant in the (110) film in-plane hysteresis loop with a square loop and higher

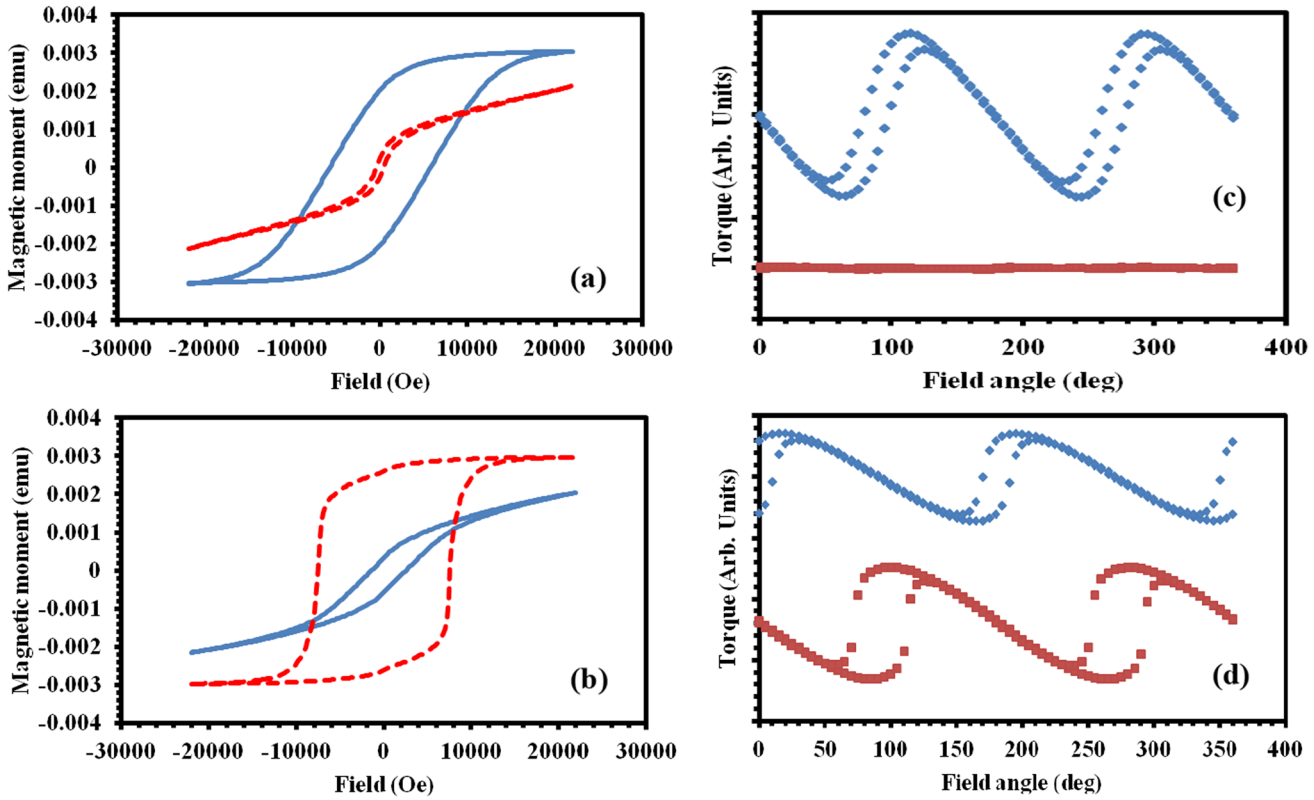

Fig. 5 Hysteresis loops for epitaxial cobalt ferrite films with **a** out-of-plane and **b** in-plane magnetic anisotropy. The red and the blue curves are the in-plane and the out-of-plane loops, respectively. Under out-of-plane anisotropy film, the out-of-plane loop is highly hysteretic and exhibits a shearing induced by the demagnetizing field, whereas the in-plane loop is almost reversible and linear and does not saturate at the maximum applied field. Extrapolating the linear behavior of the in-plane curve allows the estimation of the anisotropy field H_k at the value of 40 kOe. Under in-plane anisotropy film, the in-plane loop is square and displays a large coercivity $H_c \sim 7.5$ kOe and narrow switching between the negative and the positive magnetization states. The out-of-plane loop displays a small sheared hysteresis with linear behavior at large fields. **c** and **d** are the torque curves for out-of-plane and in-plane anisotropy films, respectively. The blue and red graphs are the out-of-plane and in-plane torque curves showing the anisotropy characteristics for both films described in the paper

remanence. (2) The singularity point representing the nucleation field which indicates the initial stage of magnetic instabilities during the magnetization reversal is well defined through a shoulder with a positive field for reversing the negatively oriented magnetization for the in-plane square loop of (110) film. However, the nucleation field is poorly defined in the perpendicular hysteresis loop of (100) film and magnetic instabilities are triggered even at negative field during the reversal mechanism of the negatively oriented magnetization. This latter result can be understood as an assisted switching mechanism for the magnetization reversal driven by the demagnetizing field, which is generated through the out-of-plane measurement geometry.

In contrast to magnetization curves measurement, the power of torque magnetometry is reflected in its ability to directly investigate the magnetic anisotropy energy and determine all its characteristics described as follows. (i) The symmetry of the magnetic anisotropy can be directly established from the periodicity of the torque curve. (ii) The anisotropy constants (first and second order) can be easily determined from the torque measurement by using Fourier analyses or Myajima method [29], whereas the anisotropy field can be precisely measured from the field dependence of the rotational hysteresis. (iii) Torque measurement facilitates the investigation of competing anisotropies [16] and can well illustrate spin reorientation phenomena occurring in magnetic systems. (iv) Torque magnetometry can sense magnetic instabilities through angular magnetic switching [30] and predict the mechanism of magnetization reversal [31, 32]. Based on all these unique characters of torque magnetometry, we performed torque curve measurement on our films to fully characterize their magnetic anisotropy energy. Figure 5c displays the out-of-plane (blue) and the in-plane (red) torque curves of (100) film measured at 20 kOe as field magnitude. In such measurement, a rotating field with a constant magnitude is applied between 0° and 360° with 5° as angle step along the clockwise and the counterclockwise rotations and the anisotropy torque is measured at each field angle. At 0° and 90° the field is aligned along the normal and parallel directions to the film plane, respectively for the

out-of-plane measurement, whereas it is parallel to [001] and [010] axes for the in-plane measurement. The out-of-plane torque curve reveals the following characteristics of the magnetic anisotropy in (100) film. (1) The 180° periodicity of the torque curve is a confirmation of the two-fold symmetry of the magnetic anisotropy energy with a uniaxial character. (2) The preferential direction of the magnetization is out-of-plane due to the reversible behavior of the torque at 0° and its zero magnitude with a negative slope at this field angle. (3) The presence of a significant amount of rotational hysteresis centered at 90° reveals that the film plane represents the hard axis of the magnetization, and the anisotropy field H_k is much larger than the measurement field (20 kOe), which corroborates the previous finding based on the extrapolation to large field of the linear reversible magnetization along the hard axis. Rotational hysteresis is an irreversible process related to the angular switching of the magnetization when the magnitude of the applied field is lower than the one of the anisotropy field [30]. The angular shearing of the rotational hysteresis is induced by the demagnetizing field through the out-of-plane measurement geometry. In contrast to a strong angular variation of the anisotropy energy through the out-of-plane torque measurement, the in-plane measurement (red curve in Fig. 5c) displays a flat reversible behavior where the in-plane torque is zero at any field angle. This latter result indicates that the in-plane anisotropy is either randomly oriented or inexistent. A random in-plane anisotropy is unconceivable under the epitaxial nature of the (100) film revealed through XRD analyses. In fact, under the uniform lattice distortion observed through the XRD symmetric scan, it is easy to predict that the anisotropy is fully out-of-plane and its in-plane component is zero. Figure 5d depicts the out-of-plane (blue graph) and the in-plane (red curve) torque curves for (110) film measured at 20 kOe. It is important to point out that for this in-plane torque measurement (red curve), at 0° and 90° the field direction is parallel to the [001] and [1$\underline{1}$0] axes, respectively. Through these torque curves, one can learn the following specific characters of the (110) film anisotropy. (1) The in-plane alignment of the anisotropy is clearly demonstrated through the hysteretic and reversible behaviors of the out-of-plane torque curve at 0° and 90°, respectively. (2) The two-fold symmetry of the in-plane torque reveals the uniaxial aspect of the in-plane anisotropy, where the easy axis is confined along [001]. (3) The large amount of rotational hysteresis in the in-plane torque in comparison to the out-of-plane one indicates that [110] (out-of-plane) and [1$\underline{1}$0] (in-plane) represent the respective intermediate and hard axes of the magnetization. The angular shearing of the rotational hysteresis for the out-of-plane torque compared to the almost square one with a vertical jump for the in-plane torque is the result of the demagnetizing field contribution to the out-of-plane measurement.

Despite a good magnetic characterization of the epitaxial films where all the characteristics of the magnetization and the anisotropy have been revealed through hysteresis loops and torque curves measurements, there is still no clear answer to the strong dependence of the magnetic viscosity on the anisotropy orientation and the slow relaxation process in perpendicular media as reported earlier. The inability of these magnetic measurements to provide a clear understanding of the relaxation results is mainly because magnetic relaxation is a purely irreversible process, whereas, in hysteresis loops and torque curves both components (reversible and irreversible) of the magnetization contribute to the measurement and cannot be separated from each other. The only way to fully comprehend and interpret the reported relaxation results is to pursue additional investigation mainly based on the magnetic characterization of the irreversible component of the magnetization. Direct current demagnetization (DCD) remanence measurement can fulfill this need since it uniquely senses the irreversible magnetization component and allows the determination of the irreversible susceptibility and the switching field distribution [33–35]. The graphs (a) and (b) of Fig. 6 represent the DCD remanence curves of both cobalt ferrite films with out-of-plane and in-plane anisotropies, respectively. Under this remanence measurement, a large negative field is first applied to saturate the film magnetization along the negative direction, then an increasing positive field is applied and removed to allow the measurement of the remanent magnetic moment at zero field. Upon removing the magnetic field, the reversible component of the magnetization disappears, whereas the remaining magnetization at zero field is purely irreversible and can be recorded at each applied positive field. Through the remanence curves (a) and (b) of Fig. 6, one can learn the following aspects of the irreversible magnetization in (100) and (110) films with out-of-plane and in-plane anisotropies, respectively. (a) Under the control of out-of-plane easy axis, the irreversible magnetization is characterized by the absence of stable negative remanent state, which typically reflects the negative saturation. Its field dependence shows a slow variation with an almost constant slope in a wide range of applied field that extends from 0 to 13 kOe before reaching the saturation at large fields. (b) The remanence coercivity H_r known as the field of zero remanence is estimated to be 6.7 kOe from Fig. 6a for the out-of-plane anisotropy film. (c) The remanence curve of the in-plane anisotropy film reveals a completely different behavior characterized by two stable irreversible magnetizations below 6 kOe and above 10 kOe, which typically represent the two saturation states along the negative and the positive directions, respectively, and an abrupt change with fast increase between 6 and 10 kOe. (d) The remanence coercivity H_r for the in-plane anisotropy film is estimated to be close to 7.5 kO and the slope of the irreversible magnetization

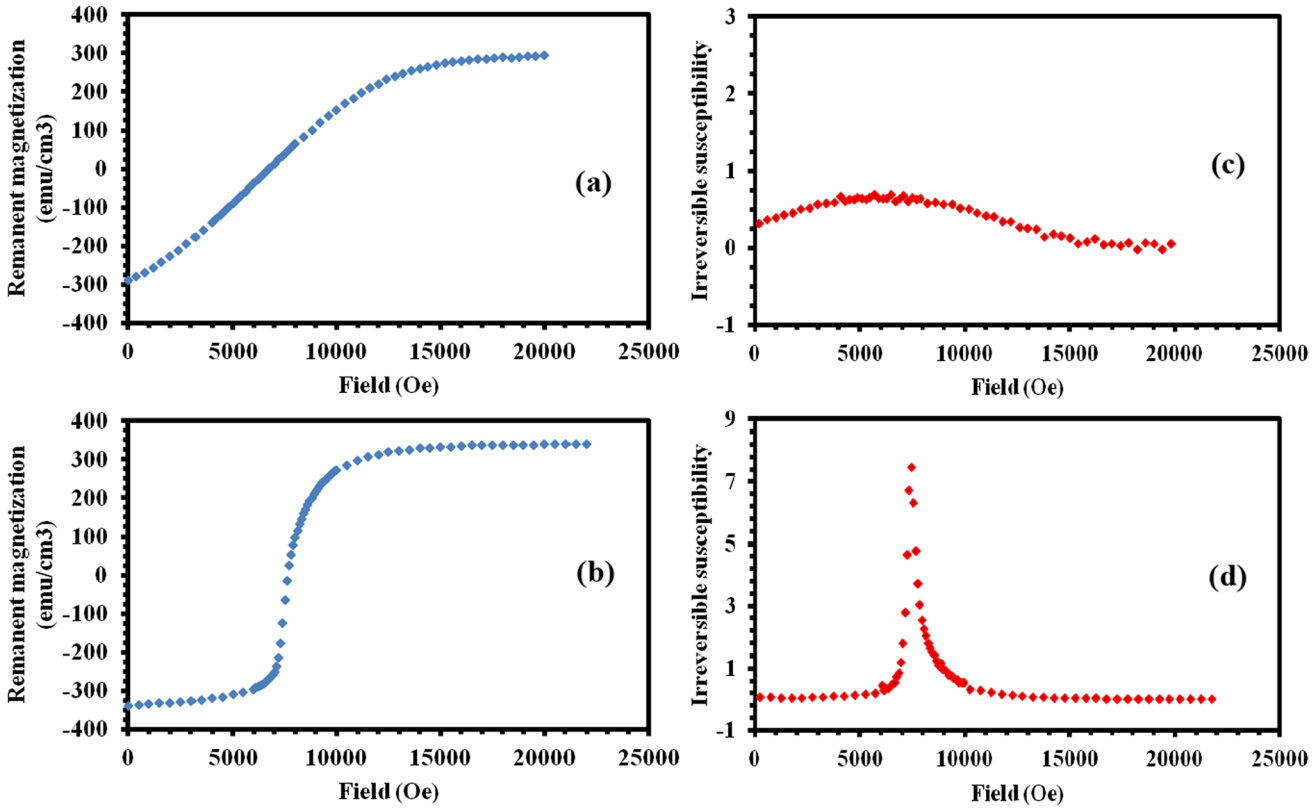

Fig. 6 DCD remanence curves for **a** out-of-plane and **b** in-plane anisotropy films showing the field dependence of the irreversible magnetization component. Under out-of-plane anisotropy, the irreversible magnetization displays a slow field variation and an almost linear behavior with nearly constant slope before reaching the saturation around 13 kOe. Under in-plane anisotropy, the irreversible magnetization displays two stable states (negative and positive) with a narrow field transition between them. Field dependence of the irreversible magnetic susceptibility for **c** out-of-plane and **d** in-plane anisotropy films, showing the irreversible magnetization process in these heterostructures. Under out-o-plane anisotropy, the irreversible susceptibility is extremely small and shows a low variation versus the applied field manifested by a broad switching field distribution. Under in-plane anisotropy, the irreversible susceptibility is extremely large at the coercivity field and the switching field distribution is very narrow

change at this field is found to be very large as illustrated by Fig. 6b. It is important to point out that the stable character of the DCD remanence in field range that extends from 0 to 6 kOe reveals that magnetic instabilities causing irreversibility in the magnetization start to develop at fields larger than 6 kOe. However, the steady increase of the irreversible magnetization with a constant slope starting from zero field for the out-of-plane anisotropy film (Fig. 6a) indicates that there is no threshold field for creating magnetic instabilities. The latter result can be understood as an assisted magnetization switching, where magnetic instabilities are triggered by the demagnetizing field H_d, which equals $-M_r$ when the external applied field is zero. This varying demagnetizing field produces a shearing in the remanence curve as reported by Fig. 6b due to the non-zero internal field H_i created by the demagnetizing field H_d for the out-of-plane anisotropy film. It is clear that the origin of the major difference between the in-plane and the out-of-plane irreversible magnetizations is the demagnetizing field, which is present under the perpendicular geometry measurement (see Fig. 7) and its varying magnitude at each applied and removed field during the DCD remanence measurement causes a continuous slow change in the irreversible magnetization through the creation of magnetic instabilities. Under in-plane anisotropy, the absence of demagnetizing field suggests that only the external applied field is behind the creation of magnetic instabilities, which require a threshold field estimated to be 6 kOe. To measure the intensity of the magnetization irreversible process, it is important to determine the irreversible magnetic susceptibility and its field dependence for both films. The graphs (c) and (d) of Fig. 6 display the irreversible magnetic susceptibility obtained from the derivative of the irreversible magnetization over the field for the out-of-plane and the in-plane films, respectively in wide range of applied field extending from 0 and 20 kOe. After scrutinizing the two graphs of the irreversible susceptibility, one can learn the drastic differences between the irreversible processes under the two anisotropy alignments, which are described as

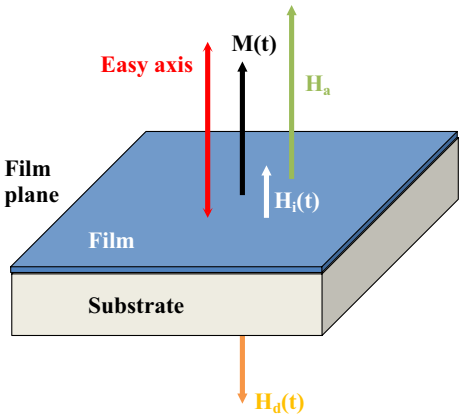

Fig. 7 Geometry of the relaxation measurement in perpendicular anisotropy film, showing the contribution of the demagnetizing field to the thermally activated process. Since the demagnetizing field $H_d(t)$ depends on the relaxing magnetization $M(t)$, the internal field H_i is also time dependent and will affect the relaxation process. In total, two sources will contribute to the time dependence of the magnetization under out-of-plane anisotropy. These two sources are the intrinsic relaxation process as in-plane media and the varying internal field over time $H_i(t)$

follow. (a) As revealed by Fig. 6c, the irreversible susceptibility for the out-of-plane anisotropy film is extremely small and never attains the value of 0.7 regardless the magnitude of the external applied field. (b) In contrast to its vanishing magnitude at large fields due to the saturation effect, the irreversible susceptibility maintains a small but non-zero value at small fields around zero. This behavior can be explained in term of the demagnetizing field, which is strongly present at zero external applied field and causes magnetic instabilities as previously discussed. (c) The very low irreversible susceptibility and its spread over all the field range are indicative of the extremely weak irreversible process and the broad switching field distribution in the out-of-plane easy axis film. (d) As illustrated by Fig. 6d, the irreversible magnetic susceptibility for the in-plane anisotropy film is equal to zero at fields lower than 6 kOe and larger than 10 kOe due to the two metastable states of the magnetization characteristic of the negative and the positive saturations. (e) The very fast variation of the irreversible susceptibility in the 6 kOe–10 kOe field range and its extremely large value that exceeds 7 at the coercivity field confirm the strong irreversible process with very narrow switching field distribution in the in-plane anisotropy film. Through all this magnetic investigation, it becomes clear that there are major differences in the magnetic irreversible process in relation to the anisotropy alignment, which can be summarized as the following. (a) The out-of-plane easy axis film displays an extremely weak irreversible process and very broad switching field distribution. (b) The irreversible process is very strong and localized in very narrow applied field range in the in-plane anisotropy film as demonstrated by its irreversible susceptibility field dependence. Since magnetic relaxation is purely irreversible process driven by thermal switching of the magnetization, it is obvious that its intensity is modulated by the irreversible susceptibility, which shows weak and strong relaxation characters for out-of-plane and in-plane anisotropy media, respectively. Moreover, the magnetic viscosity S, which represents the slope of the magnetization decay over time is expected to follow the same behavior as the irreversible susceptibility χ_{irr} at constant activation volume and magnetization according to the relation: $S = \chi_{irr} \times (kT)/(M_s \times V_{ac})$. More quantitative information about the in-plane and the out-of-plane magnetic viscosities and their relation with the irreversible susceptibility and the demagnetizing factor will be detailed in the next section through the developed analytical model.

6 Analytical modeling and relation between in-plane and out-of-plane magnetic viscosities

In this section, we aim to develop a simple model that can provide an analytical expression that relates the in-plane and the out-of-plane magnetic viscosities and corroborate the previous experimental findings, which reveal slow and fast relaxation processes in out-of-plane and in-plane media, respectively. Under this model, S_{in} and S_{out} denote the in-plane and the out-of-plane magnetic viscosities, respectively and the magnetization is assumed to obey a logarithmic decay over time as experimentally established. dM_{in} and dM_{out} represent the infinitesimal changes in the in-plane and the out-of-plane magnetization during the relaxation process and can be quantified according to the two following equations:

$$dM_{in} = -S_{in} \times d(\ln t), \tag{1}$$

and

$$dM_{out} = -S_{out} \times d(\ln t). \tag{2}$$

As depicted by Fig. 7, under a perpendicular anisotropy when an external magnetic field H_a is applied to produce a magnetization M within the medium, the magnetic structure itself generates a demagnetizing field H_d equals to $-N \times M$, where N is the demagnetizing factor, which equals 1 for a two-dimensional structure. It is obvious that the internal field H_i acting on the out-of-plane magnetic system consists of the superposition of the external applied field H_a, which is constant and the demagnetizing field

$$H_d = -M, \tag{3}$$

which is time dependent trough the relaxation of the magnetization M. The time dependent character of the internal field

$$H_i(t) = H_a - M(t), \tag{4}$$

suggests that beside the intrinsic relaxation of the out-of-plane magnetic system, an additional source is contributing to the total variation of the magnetization over time, namely driven by the non-constant internal field. Therefore, the infinitesimal variation of the magnetization of magnetic structure with an out-of-plane easy axis can be expressed as:

$$dM_{out} = dM(t) + dM(H_i). \tag{5}$$

The term $dM(t)$ represents the intrinsic magnetic relaxation, which is independent from the anisotropy alignment and can be expressed as:

$$dM(t) = dM_{in} = -S_{in} \times d(\ln t). \tag{6}$$

The component of the magnetization variation produced by the internal field can be expressed as:

$$dM(H_i) = (\partial M/\partial H_i) \times dH_i, \tag{7}$$

where

$$dH_i = (\partial H_i/\partial(\ln t)) \times d(\ln t), \tag{8}$$

Since the variation of the internal field H_i with time is established to be through the relaxing magnetization $M(t)$, the partial derivative $(\partial H_i/\partial(\ln t)$ can be expressed as:

$$(\partial H_i/\partial(\ln t) = (\partial H_i/\partial M) \times (\partial M/\partial(\ln t)). \tag{9}$$

The term $(\partial M/\partial H_i)$ in Eq. 7 represents the intrinsic irreversible susceptibility $\chi_i = \partial M/\partial H_i$, whereas the terms $(\partial H_i/\partial M)$ and $(\partial M/\partial(\ln t)$ in Eq. 9 are equal to $-N$ (demagnetizing factor) and $-S_{out}$ (magnetic viscosity). The substitution of all these terms in Eq. 5 allows us to establish a new relationship, which is:

$$-S_{out} \times d(\ln t) = -S_{in} \times d(\ln t) + (-N) \times (\chi_i) \times (-S_{out}) \times d(\ln t). \tag{10}$$

The simplification of Eq. 10 provides the final relationship between S_{in} and S_{out}, which is expressed as:

$$S_{in} = S_{out} \times (1 + N \times \chi_i). \tag{11}$$

To test the credibility of this analytical model, it is imperative to compare the experimental results and see whether they satisfy the established Eq. 11. Since both in-plane and out-of-plane magnetic viscosities are measured at the same fields, it is more convenient to compare the field dependence of the ratio S_{in}/S_{out} with that of the term $(1+N\times\chi_i)$, where the demagnetizing factor N equals 1 for the two-dimensional magnetic structure. The graphs (a) and (b) of Fig. 8 display the field dependence of the magnetic viscosities ratio (S_{in}/S_{out}) and the irreversible term $(1+\chi_i)$, respectively. These two graphs exhibit the same behavior characterized by the presence of a peak in the field range 6–10 kOe with a maximum amplitude around 7.5 kOe and a flat field dependence below 6 kOe and above 10 kOe. The agreement between the two graphs of Fig. 8 corroborates the developed analytical model under which S_{in}/S_{out} must equal the irreversible term $(1+\chi_i)$. It is important to point out that despite the good agreement between the two graphs of Fig. 8, the amplitudes of the two peaks of the two graphs are slightly different. This may be explained by the in-plane and the out-of-plane anisotropy samples investigated under this study are not 100% identical in term of microstructure and magnetic properties as demonstrated by the difference in activation volume, coercivity and remanence coercivity.

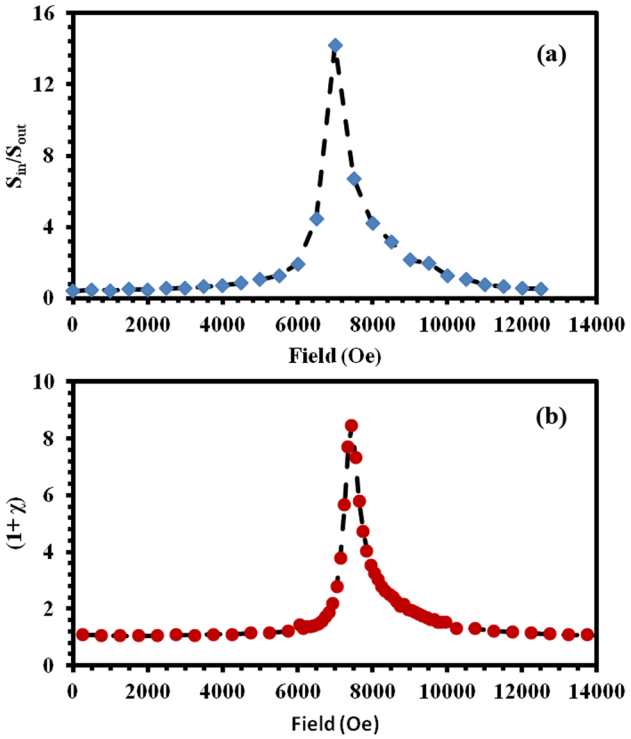

Fig. 8 Field dependence for **a** the measured magnetic viscosity ratio S_{in}/S_{out} and **b** the measured factor $(1+\chi_i)$. According to the analytical model developed in this paper, these two factors must be equal, which is well illustrated through the behavior of the two graphs of this figure. Note that the small difference between the two graphs is mainly due to the fact that S_{in} and S_{out} have been measured under two different samples with different domains structures and activation volumes, while under the model the two samples must be identical with the exception of the alignment of their magnetic anisotropy

7 Conclusions

Thermally activated magnetic switching has been investigated in epitaxial films with in-plane and out-of-plane magnetic anisotropies through magnetic relaxation measurement. It is found that while in both media the magnetization time dependence obeys a logarithmic law, the out-of-plane magnetic viscosity is extremely small and remains under 1.7 kA/m, in contrast to extremely large in-plane magnetic viscosity, which exceeds 22 kA/m at the coercivity field. The origin of the magnetization logarithmic law is a consequence of the epitaxy itself under which the film growth is initiated through random nucleation followed by islands growth and their coalescence, leading to a non-uniform size of structural domains as illustrated by HRTEM imaging. The structural domains behave like magnetic domains due to the presence of antiphase boundaries where exchange coupling is disrupted. The activation volume for both in-plane and out-of-plane easy axes films was determined and found to match the average size of the structural domains. The very slow relaxation process under out-of-plane easy axis is found to be caused by the demagnetizing field, which drastically weakens the irreversible magnetic susceptibility. A simple analytical model was developed and found to well predict and corroborate the experimental findings. The study of interest was conducted on cobalt ferrite films epitaxially grown by pulsed laser deposition on (100) and (110) MgO substrates.

Acknowledgements The authors gratefully acknowledge the financial support from the National Science Foundation under research grants NSF DMR 2055432, and DMR 2117180.

Author contributions AL designed and wrote the manuscript. He also synthesized the samples for this study, which consist of $CoFe_2O_4$ films epitaxially grown by pulsed laser deposition on (100) and (110) MgO substrates. He performed XRD, relaxation and torque measurements. FE carried out the measurement of hysteresis loops with a vibrating sample magnetometer along the directions parallel and perpendicular to the film plane. MW contributed to the TEM high resolution imaging. He edited the manuscript and provided feedback on the paper.

Data availability The data supporting the findings of the current study are available from the corresponding author upon reasonable request.

Declarations

Conflict of interest All authors certify that they have no affiliations with or involvement in any organization or entity with any financial interest or non-financial interest in the subject matter or materials discussed in this manuscript.

References

1. L. Néel, Ann. Géophys. **5**, 99–136 (1949)
2. W.F. Brown Jr., Phys. Rev. **130**, 1677 (1963)
3. R.J. Blagg, L. Ungur, F. Tuna, J. Speak, P. Comar, D. Collison, W. Wernsdorfer, E.J.L. McInnes, L.F. Chibotaru, R.E.P. Winpenny, Nat. Chem. **5**, 673–678 (2013). https://doi.org/10.1038/nchem.1707
4. R. Sessoli, D. Gattteschi, A. Caneschi, M.A. Novak, Nature **365**, 141–143 (1993). https://doi.org/10.1038/365141a0
5. S. Gómez-Coca, A. Urtizberea, E. Cremades, P.J. Alonso, A. Camón, E. Ruiz, F. Luis, Nat Commun. **1**(5), 4300 (2014). https://doi.org/10.1038/ncomms5300
6. D.A. Thompson, J.S. Best, IBM J. Res. Dev. **44**, 311 (2000)
7. D. Weller, A. Moser, IEEE Trans. Magn. **35**, 4423 (1999)
8. E.C. Stoner, E.P. Wohlfarth, Philos. Trans. R. Soc. **A240**, 599–642 (1948)
9. Th. Gerrits, H.A.M. van den Berg, J. Hohlfeld, L. Bär, Th. Rasing, Nature **418**, 509–512 (2002). https://doi.org/10.1038/nature00905
10. R. Street, J.C. Woolley, Proc. Phys. Soc. A **62**, 562 (1949)
11. A. Lisfi, S. Pokharel, A. Alqarni, O. Akioya, W. Morgan, M. Wuttig, AIP Adv. **8**, 056438 (2018)
12. D. Erdem, N.S. Bringham, F.J. Heiligtag, N. Pilet, P. Wamicke, L.J. Heyderman, M. Niederberger, Adv. Funct. Mater. **26**, 1954–1963 (2016)
13. A. Lisfi, C.M. Williams, J. Appl. Phys. **93**, 8143 (2003)
14. R.M. Bozorth, E.F. Tilden, A.J. Williums, Phys. Rev. **99**, 1788 (1955)
15. Y. Suzuki, G. Hu, R.B. van Dover, R.J. Cava, J. Mag. Mag. Mat. **191**, 1–8 (1999)
16. A. Lisfi, C.M. Williams, L.T. Nguyen, J.C. Lodder, A. Coleman, H. Corcoran, A. Johnson, P. Chang, A. Kumar, W. Morgan, Phys. Rev. B **76**, 054405 (2007)
17. A. Lisfi, S. Pokharel, L. Salamanca-Riba, M. Wuttig, J. Appl. Phys. **117**, 17B727 (2015)
18. E.P. Wohlfarth, J. Phys. F **14**, L155 (1984)
19. L. Néel, J. Phys. Rad. **12**, 339 (1951)
20. P. Bruno, G. Bayreuther, P. Beauvillain, C. Chappert, G. Lugert, D. Renard, J.P. Renard, J. Seiden, J. Appl. Phys. **68**, 5759 (1990)
21. W. Weiss, M. Ritter, Phys. Rev. B **59**, 5201 (1999)
22. J.A. Moyer, R. Gao, P. Schiffer, L.W. Martin, Sci. Rep. **5**, 10363 (2015)
23. D.T. Margulies, F.T. Parker, M.L. Rudee, F.E. Spada, J.N. Chapman, P.R. Aitchison, A.E. Berkowitz, Phys. Rev. Lett. **79**, 5162 (1997)
24. W. Eerenstein, T. Palstra, S. Saxena, T. Hibma, Phys. Rev. Lett. **88**, 247204 (2002)
25. W. Eerenstein, T. Palstra, T. Hibma, S. Celotto, Phys. Rev. B **66**, 201101 (2002)
26. T. Klemmer, D. Hoydick, H. Okumura, B. Zhang, W.A. Soffa, Scr. Metall. Mater. **33**, 1793 (1995)
27. F.E. Luborsky, J. Appl. Phys. **32**, S171 (1961)
28. D.E. Speliotis, J. Appl. Phys. **63**, 3432 (1988)
29. H. Miyajima, K. Sato, T. Mizoguchi, J. Appl. Phys. **47**, 4669 (1976)
30. A. Lisfi, S. Pokharel, W. Morgan, G. Warren, M. Wuttig, Nanotechnology **25**, 415702 (2014)
31. I.S. Jacobs, F.E. Luborsky, J. Appl. Phys. **28**, 467 (1957)
32. A. Lisfi, J.C. Lodder, IEEE Trans. Magn. **35**, 2754 (1999)
33. R.W. Chantrell, M. Fearon, E.P. Wohlfarth, Phys. Stat. Sol. (a) **97**, 213 (1986)
34. G.B. Ferguson, K. O'Grady, J. Popplewell, R.W. Chantrell, IEEE Trans. Magn. **25**, 3449 (1989)
35. A.-M. de Witte, K. O'Grady, G.N. Coverdale, R.W. Chantrell, J. Mag. Mag. Mat. **88**, 183 (1990)